J. Fluid Mech. (2005), *vol.* 541, *pp.* 203–229. © 2005 Cambridge University Press
doi:10.1017/S0022112005006208 Printed in the United Kingdom

Bubble velocities induced by trailing vortices behind neighbours

By LEEN VAN WIJNGAARDEN

J. M. Burgers Center for Fluid Mechanics, University of Twente, Enschede, The Netherlands

(Received 4 January 2003 and in revised form 5 May 2005)

Although potential flow, including viscous dissipation, explains quite well the flow around individual bubbles of about 1 mm radius rising in water, and e.g. predicts their drag quite accurately, this model cannot explain the homogeneous rise of a bubbly suspension. From numerical and analytical work it follows that eventually all bubbles cluster together. On the other hand it has been shown that velocity fluctuations of the bubbles of sufficient intensity, expressed in terms of a critical (pseudo) temperature, prevents clustering.

Bubbles with radius above 0.8 mm rising in water perform zigzag or spiralling motions. Recently experimental and numerical work has made it clear that such bubbles have a wake behind them consisting of twin vortical threads carrying vorticity of opposite sign in the direction of motion. It is the purpose of this contribution to make an estimate of the velocity fluctuations induced by these trailing vortices in neighbouring bubbles. To this end the two-threaded wake is represented as a horseshoe vortex similar to the wake behind an airfoil. A pair of bubbles is considered and first the velocity induced by the horseshoe vortex behind one of the pair at the centre of the other is calculated. After this the force exerted on the latter based on the induced velocity and on the relative velocity of the bubbles, due to hydrodynamic interaction is calculated. Then the motion of one bubble in the pair is analysed under the influence both of this force and the hydrodynamic forces already there in the absence of the horseshoe vortex. Using these results and appropriate averaging, an estimate is made of the intensity of the velocity fluctuations of bubbles, and the corresponding temperature.

1. Introduction

Numerous experiments have shown that a collection of air bubbles of about 1 mm radius rises in water as a homogeneous suspension up to a concentration by volume of 25 %, say. The average velocity of rise decreases with increasing concentration due to hydrodynamic interaction between bubbles. Attempts to describe this interaction and to derive properties of the suspension including a steady probability distribution have failed thus far. The flow around a single rising bubble of this size is well understood (Moore 1963, 1965). At the interface of the bubble with the liquid the tangential stress must be zero, as opposed to the flow around a solid body where the no-slip condition holds, and this causes a weak vorticity in the boundary layer and in a narrow wake behind the bubble. Denoting the Reynolds number of the flow around such a bubble by Re, the correction to the potential flow due to the boundary layer is of order $Re^{-1/2}$ and for the relevant Reynolds numbers negligible. Apart from this $Re^{-1/2}$ correction the flow is potential, though viscous. The drag can to leading order be derived from

https://doi.org/10.1017/S0022112005006208 Published online by Cambridge University Press

the dissipation in the viscous potential part of the flow. This model of the flow explains the rise velocity of single bubbles very well as many experiments, e.g. by Duineveld (1995), see also Magnaudet & Eames (2000), show. The next step, in the spirit of the kinetic theory of dilute gases, is to consider pairs of bubbles. Kok (1993*a*, *b*) considered pairs of rising bubbles using the same model (Kok 1993*a*) and found good agreement with experiments in Kok (1993*b*). So it is natural that Sangani & Didwania (1993) and Smereka (1993) also employed this model, that is viscous potential flow, in their numerical simulation of a large number of rising bubbles with the expectation that an initially random collection would eventually evolve into a homogeneously rising suspension. This, however did not happen. Instead, horizontal clusters are formed as time proceeds. Van Wijngaarden (1993) noted that pairs with a horizontal line connecting the centres have a high probability. He considered a suspension in which all the pairs have a horizontal line of centres and showed that no steady probability distribution exists, and that bubbles eventually cluster.

Somewhat later two papers, Yurkovetsky & Brady (1996) and Spelt & Sangani (1998) appeared describing numerical simulations in which bubbles were in addition provided with random initial impulses with a zero mean, thus representing bubble velocity fluctuations. In the latter paper viscous dissipation was also allowed for. In both simulations clustering appeared when the intensity of the fluctuations sinks below a certain critical value. It is of importance to note that the clustering in horizontal aggregates is not caused by viscous effects but is an essentially inertial effect due to hydrodynamic attraction. In a real life situation such fluctuations are absent when bubbles are released in a quiescent liquid and for that situation the simulations predict clustering, which nevertheless is not observed in experiments. So the question arises whether aspects of a real bubbly flow in quiescent water, not taken into account in the models discussed above, could provide such fluctuations.

As a candidate for such an aspect we consider here the wake behind bubbles. Up to a radius of about 0.8 mm bubbles rise rectilinearly and there is a narrow single wake containing only azimuthal vorticity. Above that size bubbles display zigzag or spiralling motion and this is accompanied by a wake consisting of two threads bearing axial vorticity. This was reported e.g. in Lunde & Perkins (1997) but studied in greater detail recently by de Vries (2001) and de Vries, Biesheuvel & van Wijngaarden (2002). In particular these authors were able to visualize the two-threaded wakes. They also measured many properties of the threads such as self-induced velocity and distance between the threads.

Figure 1 shows an experimental result by C. H. J. Veldhuis (2005, personal communication) of a spiralling bubble. Numerical calculations also have produced such wakes (Mougin & Magnaudet 2002), see figure 2. Mougin & Magnaudet (2002) find that initially zigzagging bubbles end up with a spiralling trajectory. De Vries *et al.* (2002) report that during their experiments both types of motion were found with bubbles of radius larger than 0.81 mm.

It is clear that the trailing vortices will affect the flow of suspensions. Experimental work by Cartellier & Rivière (2001) and by Risso & Ellingsen (2002) has indeed shown that, whereas in front of the bubbles in a suspension the velocity distribution agrees with what potential theory predicts, aft velocities fall off more rapidly than behind a single bubble. It is not clear why this is so but it is likely that vortices are associated with this. We do not pursue that question here but we want to analyse velocities induced in neighbouring bubbles by such two-threaded wakes. Such velocities are indeed observed in experiments by Duineveld (1994), see also Duineveld (1998), and by de Vries *et al.* (2002). Duineveld (1994) describes experiments with two bubbles

https://doi.org/10.1017/S0022112005006208 Published online by Cambridge University Press

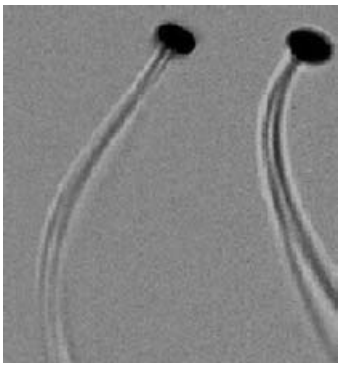

FIGURE 1. Two mutually perpendicular views of a double-threaded wake behind a nearly perfectly spiralling bubble with an equivalent radius of 1.01 mm (from an experiment by C. H. J. Veldhuis).

FIGURE 2. Isosurfaces of streamwise vorticity in the two-threaded wake behind a spiralling bubble; from the numerical simulation by Mougin & Magnaudet (2002).

rising side by side and observed that above the critical Reynolds number for path instability (in 1994 the bi-threaded wakes were not yet visualized), the two bubbles kept bouncing against each other and finally escaped from their mutual influence. Duineveld (1994, 1998) calls this 'bouncing and separation' and in Duineveld (1998) it is attributed to the action of vortices. This is in contrast to what happens below the critical Reynolds number for path instability. Then bouncing becomes weaker and weaker and ends in coalescence. De Vries *et al.* (2002) performed, apart from the experiments mentioned with single bubbles, experiments on the interaction of a single bubble with a vertical wall. In potential flow this would be equivalent to the interaction with another bubble rising at its side, but in a real fluid this is not entirely so because of different conditions at the line of symmetry. Nevertheless some correspondence may be expected. De Vries *et al.* (2002) found that at Reynolds numbers below path instability a bubble bounces a few times against the wall and finally slides along the wall. Above a certain bubble size repeated bouncing takes place over a much longer time. They write that the critical parameter "turns out to be the same critical parameter that signifies the transition from rectilinear motion to zigzagging or spiralling motion of free rising bubbles". These observations are strong indications that trailing vortices are indeed capable of inducing significant velocities in neighbours.

https://doi.org/10.1017/S0022112005006208 Published online by Cambridge University Press

Since there are differences between zigzagging and spiralling we shall focus on the latter. Of course such a motion itself implies fluctuations but these can, as we shall see, be separated from the fluctuations that one bubble induces in another.

2. The double threaded wake

Consider a bubble rising in a clean, i.e. devoid of surfactants, liquid. Numerical analysis by Mougin & Magnaudet (2002) shows that at a Reynolds number, based on diameter, of about 600 the rectilinear motion becomes unstable and a bifurcation occurs at which the linear motion changes to a zigzag motion, subsequently turning into a spiralling trajectory. The shape of the bubble at such a Reynolds number is an oblate ellipsoid. It should be noted that in the numerical work by Mougin & Magnaudet (2002) bubbles have a fixed ellipsoidal shape. In experimental work the shape is an ellipsoid also, with good accuracy, but the axes ratio varies with the Reynolds number. De Vries (2001) reports the onset of path instability at a Reynolds number of 740, slightly above that obtained by Mougin & Magnaudet (2002). The equivalent bubble radius as reported by de Vries (2001) then is 0.81 mm.

As long as the motion is rectilinear the horizontal momentum in the fluid is zero and this remains so. At instability two threads appear, bearing streamwise vorticity of equal magnitude and opposite sign, such that the momentum of the two of them together is opposite to that caused by the bubble motion. We denote the terminal rise velocity of a bubble by V, and its effective radius with a_e. In addition ρ and ν denote fluid density and kinematic viscosity respectively. In clear water V is about $0.35\,\mathrm{m\,s^{-1}}$ for bubbles with a_e of the order of 1 mm. The ratio χ between the longer and the shorter axes is usually expressed in terms of the Weber number $We = 2\rho V^2 a_e/\gamma$, γ denoting surface tension. At the experimentally observed onset of path instability, equivalent radius 0.81 mm, the Weber number is 2.7 in water. The experimental graph in Duineveld (1995) for χ as a function of We gives $\chi = 1.7$, somewhat lower than $\chi = 2.2$ found in the simulation by Mougin & Magnaudet (2002).

In de Vries (2001) it is reported that for this kind of bubble the self-induced velocity of the vorticity threads, here indicated with U, is about $0.2V$, that is approximately $7\,\mathrm{cm\,s^{-1}}$, a conclusion from numerous pictures of bubbles with their wake. Extensive measurements of trajectories of this kind of bubble were made by Ellingsen & Risso (2001). They found that the shape is approximately an oblate ellipsoid, with the shorter axis in the direction of the bubble velocity. The spiral has a frequency of about 5 Hz. It is clear that the wake described induces velocities in the adjacent fluid. If there is another bubble, its motion is affected.

We shall in the following make use of an earlier paper, van Wijngaarden (1993), henceforth denoted by VW, on the relative motion between two bubbles when the fluid motion is governed by viscous potential flow as described in the Introduction. It was shown in VW that, assuming an energy-conserving collision, the bubbles in general bounce against each other till viscosity exhausts the kinetic energy involved. We will investigate whether the trailing vortices behind the bubbles are able to supply energy to this motion. We shall make use of the circumstance that the time scale for the hydrodynamic interaction between two bubbles is a_e/V, much smaller than the time scale for the spiralling motion, which is typically 0.2 s. With bubbles of 1 mm radius and $V \cong 0.4\,\mathrm{m\,s^{-1}}$, a_e/V is 0.0025 s, two orders of magnitude smaller. So, we can assume the spiralling motion to be 'frozen' during the interaction of the test bubble with another one. The test bubble can be approached by another from many directions. Without wakes, the direction in which the line of centres is horizontal has

https://doi.org/10.1017/S0022112005006208 Published online by Cambridge University Press

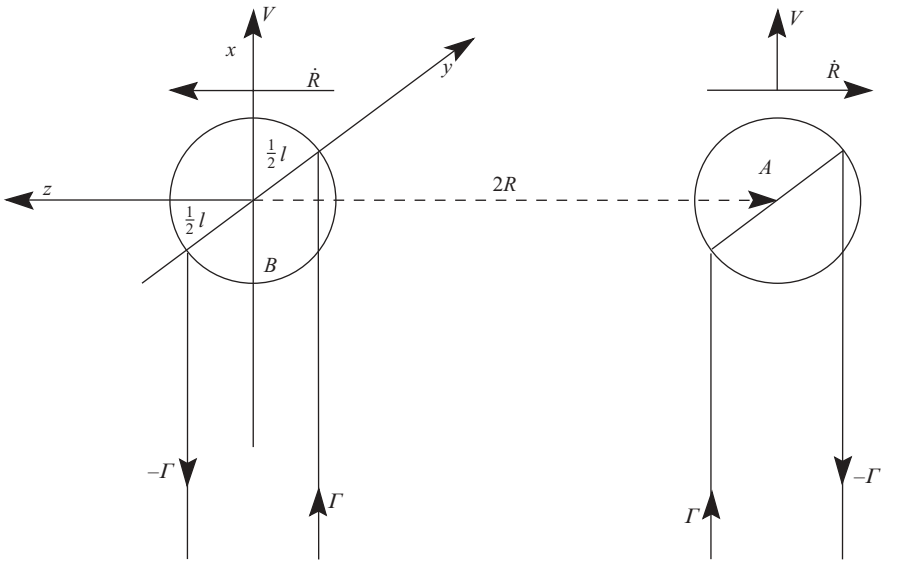

FIGURE 3. Two bubbles in spiralling motion close to another. They have a vertical velocity V, in the x-direction and a (small) sideways velocity U, mentioned in the text but not shown in the figure. Both bubbles have a wake consisting of two threads carrying vorticity of opposite sign and equal magnitude Γ. Bubble A is the test bubble and is in hydrodynamic interaction with B. The line of centres is horizontal, the separation between these centres is $2R$.

statistically a high probability, see VW (pairs with vertical line of centres rise faster and those with a horizontal one slower than a single bubble), and we will consider that configuration first. We imagine two spiralling bubbles approaching each other along a horizontal line. When both have reached their maximum (but in opposite direction) excursion and therefore minimum relative distance, their trajectories start to go in opposite directions, as sketched in figure 3. This is the moment in which we 'freeze' their spiralling motion and consider the hydrodynamic interaction. The dynamics of a pair of bubbles without trailing vortices were investigated in detail in VW. The relative velocity due to hydrodynamic interaction is of order of V, and at bouncing the relative velocity is about $0.9V$, which is much larger than U (for oblate ellipsoids it appears to be even larger, $1.5V$, see (5.6)).

When, in analysing the relative motion, we wish to add the influence of the double-threaded wake, the question arises of how to represent the wake. We choose to do this by considering it as a horseshoe vortex with straight arms, similar to the horseshoe vortex behind an aeroplane. This ignores the spiral shape of the vortices but that makes little difference in view of the relatively (with respect to the bubble radii) long wavelength, about 25 cm, of the vortical threads.

3. The force exerted by a horseshoe vortex on a bubble

In figure 3 the situation is depicted. The test bubble, bubble A, is separated from bubble B by a horizontal distance $2\boldsymbol{R}$ between the centres. Both A and B have trailing behind them a horseshoe vortex. The relative velocity due to hydrodynamic interaction between the two bubbles is $2\,\mathrm{d}\boldsymbol{R}/\mathrm{d}t$, or $2\dot{\boldsymbol{R}}$. The horizontal velocity U due to the spiralling motion is equal but opposite for the two bubbles, because A moves to

https://doi.org/10.1017/S0022112005006208 Published online by Cambridge University Press

the right and B to the left. This means that the signs of the circulation in the threads is as indicated in the figure. Note that the solenoidal property of vorticity implies a constant circulation along the threads. Let Γ be counterclockwise circulation and l the distance between the two threads behind each bubble. The rate of change $\Gamma\rho lV$ of the wake momentum equals roughly, apart from a viscous force, the rate of change of the horizontal component of the bubble impulse. If $\boldsymbol{v}$ denotes bubble velocity and $\boldsymbol{m}$ the virtual mass tensor, the bubble impulse is $\boldsymbol{m}\cdot\boldsymbol{v}$. From all observations, for example Ellingsen & Risso (2001) it follows that spiralling bubbles have the shape of an oblate ellipsoid whereby the shorter axis is in the direction of the momentary velocity. The shorter axis is oscillating around the vertical direction during the spiralling motion. In the present calculation we shall take the short axis in the vertical direction for both ellipsoidal bubbles, which are axisymmetric with respect to this axis.

We need to know some hydrodynamic properties of such ellipsoids, in particular added mass, drag and dipole strength in uniform flow. Added mass values can be obtained from the potential flow around an ellipsoid as given in Milne-Thomson (1968, pp. 501, 534). For motion in the direction of the minor axis and major axis respectively we have

$$m_1 = \rho Y Q_1(\chi), \tag{3.1}$$

$$m_2 = \rho Y Q_2(\chi). \tag{3.2}$$

Here Y is the volume of a bubble. For spheres both Q_1 and Q_2 have the value 0.5. Relations between the Q and χ are given and/or derived in Appendix C.

Next we consider the drag. For motion in the vertical direction the drag has been obtained by Moore (1965) in the form

$$D_1 = 12\pi\mu a_e V G(\chi) \tag{3.3}$$

where μ is the dynamic liquid viscosity, a_e the effective bubble radius defined by

$$Y = \tfrac{4}{3}\pi(a_e)^3 \tag{3.4}$$

and $G(\chi)$ is found from equating the dissipation to VD_1. In our calculation the vertical drag is balanced by the buoyancy force on the ellipsoids. Since we are in particular interested in the relative motion we need the drag in the horizontal direction. This has not been calculated by Moore (1965) nor by anybody else. For the present and future purposes Veldhuis & van Wijngaarden (2005) performed the corresponding calculation to determine the drag F_1 of an ellipsoid, symmetrical about the short, vertical, axis when the ellipsoid moves in horizontal direction with velocity $\dot{\boldsymbol{R}}$. The result is

$$F_1 = -12\pi\mu a_e \,\mathrm{d}R/\mathrm{d}t\, J(\chi). \tag{3.5}$$

The relation between $J(\chi)$ and χ is

$$J = \frac{2(\chi^2-1)^{3/2}\{(\chi^2-2)(\chi^2-1)^{1/2} + \chi^4 \sec^{-1}\chi\}}{3\chi^{2/3}\{(2\chi^2-1)(\chi^2-1)^{1/2} - \chi^2 \sec^{-1}\chi\}^2}.$$

The function $J(\chi)$ is drawn in figure 4. Just like $G(\chi)$ it takes the value unity for $\chi = 1$. For the moderate values of χ which are of interest to us here, the sideways drag is below that of a sphere with the same volume.

A third property of importance is the dipole strength for motion in the directions of the minor and major axes. Let these be M_1 and M_2 respectively. They are obtained

https://doi.org/10.1017/S0022112005006208 Published online by Cambridge University Press

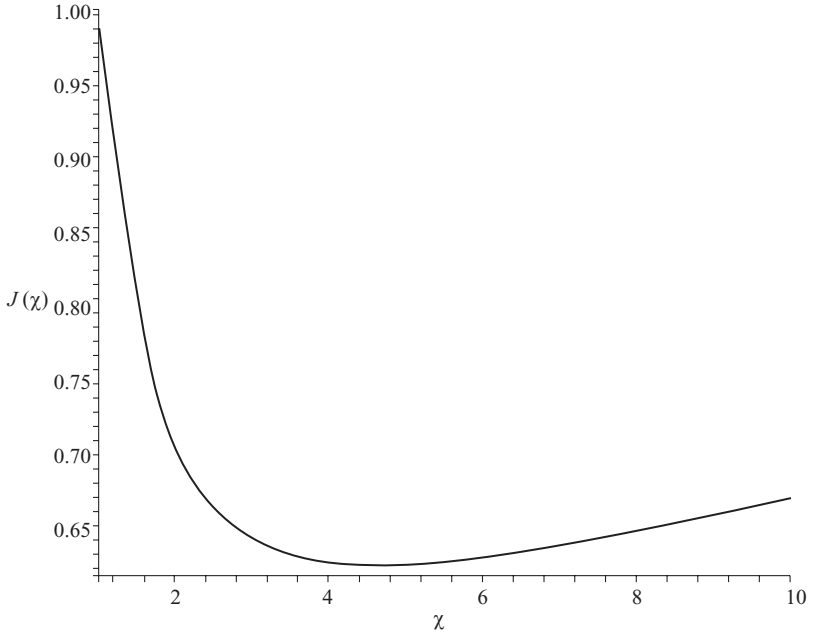

FIGURE 4. The viscous drag of an axisymmetric ellipsoid moving in the direction of the longer axis is $F_1 = -12\pi\mu a_e(\mathrm{d}R/\mathrm{d}t)J(\chi)$, see equation (3.5). $J(\chi)$ is shown.

from the relation which, both for rigid and for deforming bodies, exists between dipole strength and impulse, see e.g. Benjamin & Ellis (1990). For a body moving with velocity $\boldsymbol{v}$ this relation is

$$4\pi\boldsymbol{M} = Y\boldsymbol{v} + \boldsymbol{m}\cdot\boldsymbol{v}/\rho. \tag{3.6}$$

Using (3.1) and (3.2) for m_1 and m_2 we obtain from this relation

$$4\pi M_1 = YV\{1 + Q_1(\chi)\}, \tag{3.7}$$

$$4\pi M_2 = Y|\dot{\boldsymbol{R}}|\{1 + Q_2(\chi)\}. \tag{3.8}$$

In the situation of figure 3 there is a second bubble in the vicinity of the test bubble. The hydrodynamic properties discussed above are affected by its presence. For spherical bubbles this was investigated in detail in van Wijngaarden (1976) and van Wijngaarden & Kapteyn (1990). The added mass of each of the bubbles in a pair is larger by a factor $\{1 + 3/16(a/R)^3\}$, and the drag D_1 by a factor $\{1 + 1/8(a/R)^3\}$. With ellipsoids the numerical coefficients will be different but the variation as $(a_e/R)^3$ remains. We shall neglect this small quantity.

Recently Legendre, Magnaudet & Mougin (2003) carried out a full Navier–Stokes solution for the same situation as considered here: two bubbles rising side by side in clean water, but at Reynolds numbers (the maximum value in their work is 500) below the threshold where zigzag and spiralling occurs. Nevertheless there is a wake and there are boundary layers, carrying vorticity. The results obtained (p. 145 of Legendre *et al.* 2003) "confirm that added-mass effects are not altered by viscous effects even in a bounded flow domain". We can therefore use the results for added mass from potential flow with confidence.

In addition to the slow, of order of $\mathrm{cm\,s^{-1}}$, velocity associated with the spiralling motion, which we shall ignore as explained before, the bubbles have a relative velocity

https://doi.org/10.1017/S0022112005006208 Published online by Cambridge University Press

$2\mathrm{d}\boldsymbol{R}/\mathrm{d}t$, or $2\dot{\boldsymbol{R}}$, caused by hydrodynamic interaction. It should be emphasized that this relative motion does not change the net momentum in the liquid and is quite different from the spiralling motion exhibited by each of the bubbles alone.

We now form the force balance in the horizontal direction on the test bubble. The drag is given by (3.5), and all the other forces are obtained from the general relationship

$$\boldsymbol{F} = \{-4\pi\rho \boldsymbol{M}\cdot\nabla\boldsymbol{u}\}_{centre\ of\ ellipsoid}, \tag{3.9}$$

see e.g. Landweber & Miloh (1980), where we restrict consideration to dipole forces. In this relation $\boldsymbol{u}$ is the fluid velocity induced by bubble B in the centre of the ellipsoid A. First we consider the velocity induced by the dipole in B. The corresponding force and its ramifications for the dynamics of a bubble pair was investigated in VW. For an oblate axisymmetric ellipsoid it is, using (3.6)–(3.9),

$$F_0 = -\frac{\pi\rho a_e^6 V^2}{12R^4}(1+Q_1)^2. \tag{3.10}$$

For a sphere $Q_1 = 0.5$ and the numerical factor on the right-hand side of (3.10) becomes 3/16, as in VW. In addition there are now the forces due to the horseshoe vortex behind B. In determining these, we may neglect the influence which the horseshoe vortex behind A exerts on its counterpart behind B, for the following reasons. First we consider the recent numerical simulation of Legendre *et al.* (2003), mentioned above, in which the same configuration as here is simulated, two bubbles rising side by side, but at Reynolds numbers below the threshold where spiralling or zigzagging occurs, and using the full Navier–Stokes equations. There are wakes behind the bubbles, but without horseshoe vortices. The maximum Reynolds number is 500 in their study and they report that "at leading order the second bubble does not affect the vorticity distribution and the iso-contours would be almost identical to those if the bubble were alone". Second, this is also the case for Reynolds numbers at which spiralling occurs, as is made plausible as follows. Vortices move, by Helmholtz's laws, with the local velocity. In a frame moving with the vertical rise velocity V this is, for a bubble alone, the velocity associated with its spiralling motion. In the presence of a second bubble there is in addition the velocity induced by the latter. A calculation, given in Appendix B, shows that at a distance $3a_e$ between the centres, the velocity induced by the horseshoe vortex behind A in the arms of its counterpart behind B, is only $0.04U$. This means that the displacement of vortex B by A after 20 oscillations with period a_e/V is very small, $0.16a_e$. In the situation of figure 3 such an induced velocity would be the same on corresponding points of both arms. With an arbitrary orientation of the horseshoe with respect to the line of centres, they are different causing a change in the orientation. Such a change is small however and moreover accounted for by the averaging over all possible orientations which we shall eventually make.

We proceed now by calculating the force $\boldsymbol{F}_2$ induced by the horseshoe behind B as given in (3.9) with $\boldsymbol{M}$ the dipole given in (3.7) and (3.8). An additional force is on the image in A of the horseshoe vortex behind B. We shall come to that in § 4.

The velocity field induced by a horseshoe vortex can be found in several textbooks on hydrodynamics. We use Milne-Thomson (1952, p. 175). With an x, y, z frame for bubble B such that the arms of the horseshoe with circulation Γ and $-\Gamma$ are along $-\infty < x < 0$, $y = l/2$, $z = 0$ and $-\infty < x < 0$, $y = -l/2$, $z = 0$, the bound vortex is along $x = 0$, $l/2 \geqslant y \geqslant -l/2$, $z = 0$. In this configuration the line of centres is along the negative z-axis and the centre of bubble A at $0, 0, -2R$. Then the velocity components

https://doi.org/10.1017/S0022112005006208 Published online by Cambridge University Press

induced at x, y, z by the horseshoe are

$$u_x = -\frac{\Gamma z}{4\pi(x^2+z^2)}\{r(x,-y,z)(\tfrac{1}{2}l-y)+r(x,y,z)(\tfrac{1}{2}l+y)\}, \tag{3.11}$$

$$u_y = -\frac{\Gamma z}{4\pi\{z^2+(\frac{1}{2}l+y)^2\}}\{1-xr(x,y,z)\}+\frac{\Gamma z}{4\pi\{z^2+(\frac{1}{2}l-y)^2\}}\{1-xr(x,-y,z)\}, \tag{3.12}$$

$$u_z = -\frac{\Gamma(\frac{1}{2}l+y)}{4\pi\{z^2+(\frac{1}{2}l+y)^2\}}\{1-xr(x,y,z\}-\frac{\Gamma(\frac{1}{2}l-y)}{4\pi\{z^2+(\frac{1}{2}l-y)^2\}}\{1-xr(x,-y,z\} + \frac{\Gamma x}{4\pi(x^2+z^2)}\{r(x,-y,z)(\tfrac{1}{2}l-y)+r(x,y,z)(\tfrac{1}{2}l+y)\}. \tag{3.13}$$

In these expressions $r(x,\pm y,z)$ is shorthand for $1/\{(x^2+(l/2\pm y)^2+z^2)\}^{1/2}$. For the force on the ellipsoid we now use (3.9). We see that there are components in all three directions. Here we concentrate on the $\boldsymbol{R}$-direction. It is interesting, though, to note that apart from a central force there is also a force normal to the plane through the vertical and $\boldsymbol{R}$. Often, see e.g. Stewart (1995), bubbles have been observed darting around each other. That cannot happen within potential flow theory but as we see, vortices cause it. In this paper we focus on the relative radial motion and therefore consider the z-component of (3.9). $\boldsymbol{R}$ points in the negative z-direction, test bubble A moves in the negative z-direction relative to bubble B, with velocity $-2|\dot{\boldsymbol{R}}|$, and velocity $-|\dot{\boldsymbol{R}}|$ with respect to the liquid, therefore $\boldsymbol{M}\cdot\boldsymbol{e}_z=-M_2$ where M_2 is given in (3.8). Likewise in vertical, x, direction, with M_1 given in (3.7), $\boldsymbol{M}\cdot\boldsymbol{e}_x=M_1$. Here $\boldsymbol{e}_x$ and $\boldsymbol{e}_z$ are unit vectors in the x- and z-direction respectively. Using these values and the velocity components given in (3.11)–(3.13) evaluation of (3.9) gives

$$\begin{aligned}\boldsymbol{F}_2\cdot\boldsymbol{e}_z &= (1+Q_2)\rho Y|\dot{\boldsymbol{R}}|\frac{\partial}{\partial z}(u_z)_{0,0,-2R}-(1+Q_1)\rho YV\frac{\partial}{\partial x}(u_z)_{0,0,-2R}\\ &= F_{2,1}+F_{2,2} = -\rho(1+Q_2)Y\Gamma l\frac{R|\dot{\boldsymbol{R}}|}{4\pi(4R^2+\frac{1}{4}l^2)^2}\\ &\quad -\rho(1+Q_1)Y\Gamma l\frac{V}{4\pi(4R^2+\frac{1}{4}l^2)^{1/2}}\left\{\frac{1}{4R^2}+\frac{1}{4R^2+\frac{1}{4}l^2}\right\}.\end{aligned} \tag{3.14}$$

The forces indicated above by $F_{2,1}$ and $F_{2,2}$ have a negative sign, which means that they are felt by bubble B as repulsive. It is perhaps helpful to remind the reader that the sign of these and similar forces on a dipole can be checked as follows: the source in a dipole prefers to swim against the local stream but the sink prefers to go with it. Take for example $F_{2,1}$. The velocity induced by the horseshoe is negative. The sink–source direction is the negative z-direction, so the outward force on the sink is stronger than the inward force on the source.

We can simplify (3.14) by observing that, since bubbles cannot overlap, $R\geqslant a$. The measurements by de Vries (2001) show that l is of order a_e, and we shall in the following use his observation that

$$l\approx 0.6a_e. \tag{3.15}$$

https://doi.org/10.1017/S0022112005006208 Published online by Cambridge University Press

This means that we can safely neglect $l^2/4$ with respect to $4R^2$, which simplifies the forces in (3.14) to

$$F_{2,1} = -\frac{\rho(1+Q_2)Y\Gamma l}{16\pi R^3}|\dot{\boldsymbol{R}}|, \tag{3.16}$$

$$F_{2,2} = -\frac{\rho(1+Q_1)Y\Gamma l}{16\pi R^3}V. \tag{3.17}$$

The circulation Γ of the threads in the bubble wake can be determined from the self-induced velocity U of the threads. From many observations this was reported by de Vries (2001) to be $0.1V$–$0.2V$. The relation between Γ and U is

$$\Gamma = 4\pi l U. \tag{3.18}$$

Inserting this into (3.16) and (3.17) and taking $U = 0.2V$, we obtain

$$F_{2,1} = -(1+Q_2)\rho Y l^2 \frac{V|\dot{\boldsymbol{R}}|}{20R^3}, \tag{3.19}$$

$$F_{2,2} = -(1+Q_1)\rho Y l^2 \frac{V^2}{20R^3}. \tag{3.20}$$

At this stage we note two things about these forces. First, by inserting numerical values for the various symbols, and subsequent comparing with the primary attractive force F_0 in (3.10) and the viscous force F_1 in (3.5), it appears that the forces due to the vortices, as given in (3.19) and (3.20), are much smaller than the attractive force but comparable with the frictional force. This is promising since overcoming frictional force may maintain the velocity fluctuations. A second remark concerns the dependence on the distance $2R$ between the centres. F_0 falls off like R^{-4}. The forces due to the wake, in contrast, fall off as R^{-3}. This is explicitly shown here for the horizontally aligned relative positions, but holds, as is easily seen, for a general case as well.

In the above calculation we have considered the line of centres to be along the z-axis of the frame attached to the horseshoe vortex. For later use we include here the more general case in which there is an arbitrary angle, ψ, between the line connecting the corner points of the horseshoe and the line of centres of the two bubbles. In figure 5 are sketched, as seen from above, these corner points with the directions of the circulation about the two arms, at a distance l, and the centre of bubble A. The middle of the line connecting the corner points is at a distance $2R$ from A, the corner points themselves at distances $2R_1$ and $2R_2$ respectively. With reference to this figure it is easy to see that, with σ_1 and σ_2 as indicated, the velocity u_R in the direction of R induced in A equals $\Gamma/8\pi\{\sin\sigma_1/R_1 + \sin\sigma_2/R_2\}$. Since in our application $R \geqslant a_e$ and $l \approx 0.6a_e$, $l/4R$ is smaller than 0.15. From figure 5 we see that

$$R_1^{-1} = R^{-1}\{1 - l/4R\cos(\sigma_1+\psi_1)\} + O(l/4R)^2 \quad \text{and} \quad R_2^{-1} = R^{-1}\{1 + l/4R\cos(\sigma_1+\psi_1)\}.$$

Both $\sin\sigma_1$ and $\sin\sigma_2$ are of order $l/4R$, so if we neglect the square of this small quantity, we may write

$$u_R = \frac{\Gamma}{4\pi R}\sin\left(\frac{\psi_2-\psi_1}{2}\right). \tag{3.21}$$

Now twice the area of the triangle AB_1B_2 in figure 5 is both $2\boldsymbol{R}\times\boldsymbol{l} = 2Rl\sin\psi$ and $2\boldsymbol{R}_1\times 2\boldsymbol{R}_2 = 4R^2\sin(\psi_2-\psi_1)$, from which it follows that $\sin(\psi_2-\psi_1) = l/2R\sin\psi$,

https://doi.org/10.1017/S0022112005006208 Published online by Cambridge University Press

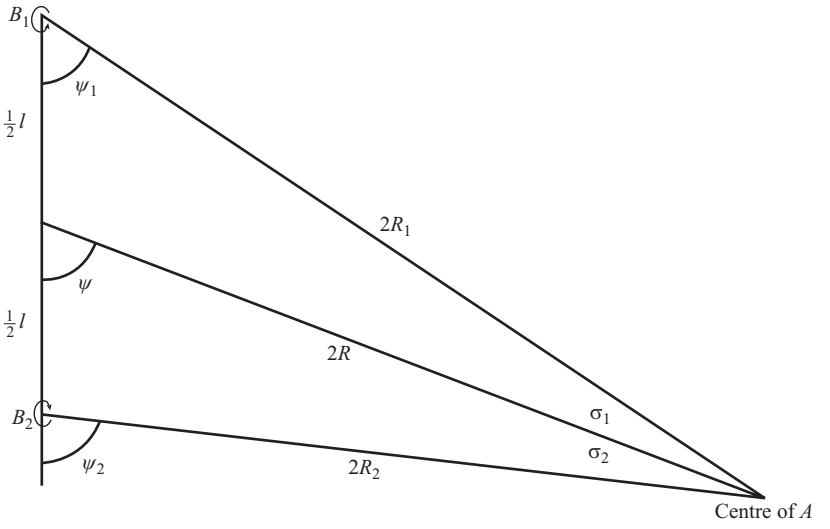

FIGURE 5. The two arms of the horseshoe vortex trailing behind bubble B, parallel to the x-axis, cut through the plane of the figure in B_1 and B_2. The line connecting the centres of bubble A and bubble B makes an angle ψ with the y-axis. The figure is an illustration of the calculation of the velocity which the horseshoe vortex induces in the centre of bubble A.

whence (3.21) becomes

$$u_R = \frac{\Gamma l \sin\psi}{8\pi R^2}. \tag{3.22}$$

In the calculation earlier in this section we have considered the case $\psi = \pi/2$.

Before proceeding with the dynamics of the interaction, we must turn our attention to the forces exerted on the images, in bubble A, of the horseshoe behind bubble B.

4. Force exerted on the image vorticity

For the determination of the force on the image vorticity in bubble A we will treat both bubbles as spherical. It will turn out that this force is small with respect to $\boldsymbol{F}_2$ as determined in the previous Section. Since the oblate ellipsoid changes only the shape and not the strength of the image vorticity this makes no significant difference. In a beautiful paper Lighthill (1956) showed that the image of a vortex filament $\Gamma\,\mathrm{d}\boldsymbol{s}$ located at a distance $\boldsymbol{r}$ from the centre of a sphere with radius a is located in a^2/r and consists of two elements. If $\mathrm{d}\boldsymbol{s} = \mathrm{d}\boldsymbol{s}_t + \mathrm{d}\boldsymbol{s}_r$, the subscripts denoting tangential and radial direction respectively, then the image consists first of an element $-\Gamma a/r\,\mathrm{d}\boldsymbol{s}_t$ and an element $\Gamma a/r\,\mathrm{d}\boldsymbol{s}_r$. This is not all. To ensure that the image vortex field is solenoidal, there is in addition a vortex sheet bounded by the image element and by the lines connecting the beginning and end points with the origin of the sphere. The circulation around this sheet accounts for the difference between the circulation at the begin point and the end point of the image element. Dhanak (1981) used this result to determine the image of a line vortex in a sphere. Let this line vortex have a circulation Γ and be located, in terms of the frame of our previous section, in $-\infty < x < \infty$, $y = 0$, $z = 0$. The centre of the sphere is at $0, 0, -2R$, see figure 6. The result of Dhanak's analysis is that the image consists in the first place of a circular vortex ring with radius $a^2/4R$ and centre, see figure 6, at $0, 0, -2R + a^2/4R$. The image of a point $\boldsymbol{r}$ on the line vortex is at a^2/r on the vortex ring and the circulation

https://doi.org/10.1017/S0022112005006208 Published online by Cambridge University Press

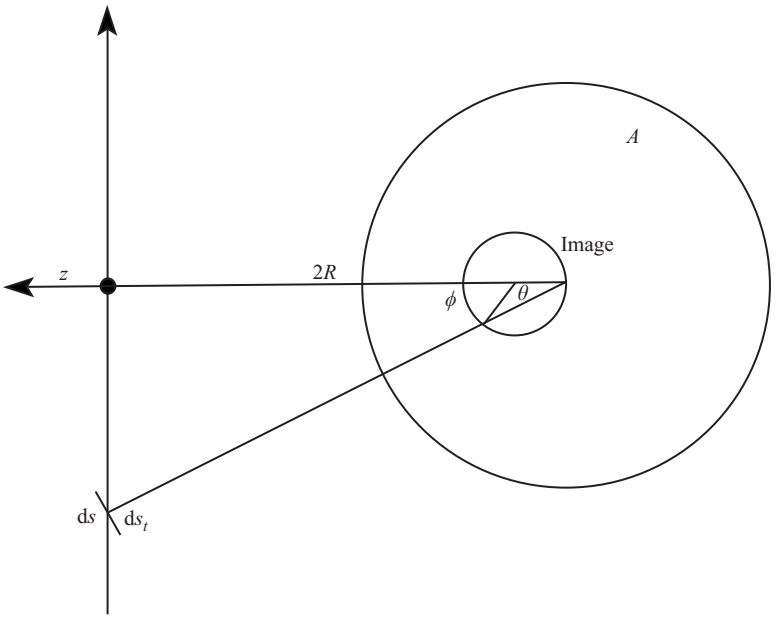

FIGURE 6. The image of a vortex line, along the x-axis, in sphere A. As explained in the text the image consists in the first place of a vortex ring with centre at $0, 0, -2R + a^2/4R$. The difference between the circulation associated with r and $r + \mathrm{d}r$ is $\Gamma\,\mathrm{d}r/a$. Further, the surface bounded by this vortex ring is a vortex sheet, needed in order to make the vorticity solenoidal.

of an element on this ring is $\Gamma r/a$. This obviously varies along the vortex ring and to ensure that the vorticity is solenoidal an additional vortex sheet is needed. Let the angle between $\boldsymbol{e}_r$, a unit vector in the $\boldsymbol{r}$-direction, and the z-axis (see figure 6) be θ, then $r = 2R/\cos\theta$. The difference $\mathrm{d}\Gamma$ between the circulation at points on the vortex ring associated with r and $r + \mathrm{d}r$ is $\Gamma\,\mathrm{d}r/a$ or

$$\mathrm{d}\Gamma = \frac{2R\Gamma\sin\theta\,\mathrm{d}\theta}{a\cos^2\theta}.$$

The circulation of the part of the vortex sheet bounded by this piece of the vortex ring and the lines connecting its ends with the origin must be equal and opposite to this. The associated vorticity is in the $\boldsymbol{r}$-direction. Since s measured along the vortex line can be written as $s = 2R\tan\theta$, we have along the sheet

$$\mathrm{d}\Gamma = \Gamma\,\mathrm{d}s\sin\theta/a = \Gamma\,\mathrm{d}s_r/a. \tag{4.1}$$

With help of this result we can now find the image of the horseshoe vortex. The two arms of the horseshoe are semi-infinite and hence the image of each of these is a semicircular vortex ring. One of these is in the plane through the origin of the sphere and the line $-\infty < x < 0$, $y = -l/2$, $z = 0$, the other in the plane through the origin and the line $-\infty < x < 0$, $y = l/2$, $z = 0$. These planes are perpendicular to the plane $x = 0$, and are at an angle $\tan^{-1} l/4R$ and $-\tan^{-1} l/4R$ with the (x, z)-plane respectively. The surfaces bounded by the semicircles are vortex sheets with circulation as in (4.1), each with the appropriate sign of Γ.

We should now calculate the force exerted on these rings and sheets at bubble A by the horseshoe vortex behind bubble B. We shall do this in Appendix A. It turns out

https://doi.org/10.1017/S0022112005006208 Published online by Cambridge University Press

that this forms a small fraction of the forces given on the right-hand sides of (3.19) and (3.20) and we shall neglect it in the following.

5. Dynamics of relative motion

We collect the forces in the z-direction on bubble A. In addition to the forces F_0 and F_1 defined in (3.10) and (3.5) respectively, we have the repulsive forces in (3.19) and (3.20). Remembering that $\boldsymbol{R}$ points in the negative z-direction, we obtain the equation of motion valid when the motion caused by the interaction is with increasing R:

$$\rho Y Q_2 \frac{\mathrm{d}^2 R}{\mathrm{d}t^2} = -12\pi\mu a_e \frac{\mathrm{d}R}{\mathrm{d}t} J(\chi) - \frac{(1+Q_1)^2}{12R^4}\pi\rho(a_e)^6 V^2 + \frac{(1+Q_2)\rho Y l^2 V}{20R^3}\frac{\mathrm{d}R}{\mathrm{d}t} + \frac{(1+Q_1)\rho Y l^2 V^2}{20R^3}. \tag{5.1}$$

The quantities Q_1, Q_2 and J in (5.1) are all functions of the axes ratio χ. We now make the calculation more specific by choosing a value of χ. We take a bubble with an effective radius of about 1 mm. Then, according to the measurements by Duineveld (1995), the rise velocity is about $0.35\,\mathrm{m\,s^{-1}}$ and χ is about 2. This value is therefore representative for the bubbles of interest here and we shall use it in the following. Using the data collected in Appendix C for the Q and figure 4 for J, we have

$$Q_1(2) = 1.17, \quad Q_2(2) = 0.30, \quad J(2) = 0.70. \tag{5.2}$$

We insert these values into (5.1), divide each term by $\rho Y Q_2$ and introduce the relaxation time τ by

$$\tau = \frac{\rho Q_2 Y}{12\pi\mu a_e J} = \frac{a_e^2}{21\nu}, \tag{5.3}$$

to obtain

$$\frac{\mathrm{d}^2 R_o}{\mathrm{d}t^2} = -0.98\frac{a_e^3 V^2}{R_o^4} + 0.36\frac{l^2 V^2}{R_o^3} + \left(-\tau^{-1} + 0.22\frac{l^2 V}{R_o^3}\right)\frac{\mathrm{d}R_o}{\mathrm{d}t}. \tag{5.4}$$

In this equation we have added the subscript o to indicate that the outgoing motion of bubble A is considered. The bubble has an initial velocity and is decelerated by the attractive force represented by the first term on the right-hand side and the frictional force, but sustained by the forces due to the horseshoe vortex. Eventually the bubble comes to rest, in a time of order a_e/V, and the inward motion starts. The force exerted by the horseshoe vortex on the radial dipole is now attractive, and the source in front 'swims' against the oncoming stream caused by the arms of the horseshoe, whereas the force on the vertical dipole keeps the same sign, and is repulsive. Hence for the incoming motion we obtain, adding the subscript i to R to indicate that the incoming motion is concerned,

$$\frac{\mathrm{d}^2 R_i}{\mathrm{d}t^2} = -0.98\frac{a_e^3 V^2}{R_i^4} + 0.36\frac{l^2 V^2}{R_i^3} + \left(-\tau^{-1} + 0.22\frac{l^2 V}{R_i^3}\right)\frac{\mathrm{d}R_i}{\mathrm{d}t}. \tag{5.5}$$

The equations for the in and out movement are the same, as we see. We must keep in mind however that $\mathrm{d}R_o/\mathrm{d}t$ is positive and $\mathrm{d}R_i/\mathrm{d}t$ negative.

In VW the terms involving l^2 are absent. Solving the remainder of the above equations for $\tau \to \infty$ shows that the bubbles keep oscillating with respect to each other, assuming elastic bounces. We denote by R_m the maximum value reached by R during

https://doi.org/10.1017/S0022112005006208 Published online by Cambridge University Press

an oscillation. The velocities during the oscillations are

$$\frac{\mathrm{d}R_o}{\mathrm{d}t} = -\frac{\mathrm{d}R_i}{\mathrm{d}t} = \left\{0.67\frac{a_e^3V^2}{R_m^3}\left(\frac{R_m^3}{R^3}-1\right)\right\}^{1/2}. \tag{5.6}$$

The time scale of this motion is a_e/V, which is of order of 1 ms. On the scale of the relaxation time τ, which is at least an order of magnitude larger, R_m becomes smaller and smaller, according to (see VW)

$$\left\{1-(a_e/R_m)^{1/2}\right\}/\left\{1-(a_e/R_m)_{t=t_0}\right\} = \exp -(t-t_0)/\tau.$$

With $a_e = 1\,\mathrm{mm}$, $V = 0.35\,\mathrm{m\,s^{-1}}$, $\nu = 0.8\times10^{-6}\,\mathrm{m^2\,s^{-1}}$ we have $\tau = 0.05\,\mathrm{s}$ and $a_e/V = 0.003\,\mathrm{s}$. This means, with a view to the above relation, that after about 20 oscillations the relative motion with time scale a_e/V is exhausted, because by that time $R_m \sim a_e$. The ratio between the time scales involved, $V\tau/a_e$, can be written as $Re/36$, where Re is the Reynolds number

$$Re = 2Va_e/\nu. \tag{5.7}$$

In our case $Re = 870$. Kumaran & Koch (1993), in connection with a study on bubble coalescence, calculated numerically the trajectories of two bubbles rising side by side at a smaller Reynolds number of 400, and their figure 2 shows that the oscillation discussed here ceases after roughly ten oscillations.

It is our intention to see what changes the two terms containing l^2, that is the terms representing the forces by the horseshoe vortices, bring. We start with the inward motion at $R = R_m$. We write (5.5) as

$$\frac{1}{2}\frac{\mathrm{d}}{\mathrm{d}R_i}\left(\frac{\mathrm{d}R_i}{\mathrm{d}t}\right)^2 = \frac{\mathrm{d}}{\mathrm{d}R_i}\left(0.33\frac{a_e^3V^2}{R_i^3}-0.18\frac{l^2V^2}{R_i^2}\right)+\left(0.22\frac{l^2V}{R_i^3}-\tau^{-1}\right)\frac{\mathrm{d}R_i}{\mathrm{d}t}.$$

We integrate between $R_i = R_m$ where $\mathrm{d}R_i/\mathrm{d}t = 0$ and $R_i = a_e$, where the maximum radial velocity, $-W$, $W \geqslant 0$, say, is reached. This gives

$$\frac{1}{2}W^2 = 0.33V^2\left(1-\frac{a_e^3}{R_m^3}\right)-0.18V^2\left(\frac{l^2}{a_e^2}-\frac{l^2}{R_m^2}\right)+\int_{R_m}^{a_e}\left(0.22\frac{Vl^2}{R_i^3}-\tau^{-1}\right)\frac{\mathrm{d}R_i}{\mathrm{d}t}\mathrm{d}R_i. \tag{5.8}$$

The value of W is mainly determined by the attractive force exerted by B, and a little reduced by the second term at the right-hand side of (5.8). The other force from the horseshoe, that in the integral, tends to increase W, but is counteracted by viscosity. We assume the collision between A and B to be elastic such that at the rebound bubble A starts with $\mathrm{d}R_o/\mathrm{d}t = W$. In the absence of the horseshoe vortex the two bubbles reach a final distance apart which is less than $2R_m$, because of viscous dissipation. With the vortex it might be larger, equal to or smaller than $2R_m$. We call this distance $2R^{\#}$. Operating on (5.4) in the same way as we did on (5.5), now integrating between $R_o = a_e$ and $R_o = R^{\#}$, we obtain

$$-\frac{1}{2}W^2 = 0.33V^2\left(\frac{a_e^3}{(R^{\#})^3}-1\right) - 0.18V^2\left(\frac{l^2}{(R^{\#})^2}-\frac{l^2}{a_e^2}\right)+\int_{a_e}^{R^{\#}}\left(0.22\frac{Vl^2}{R_o^3}-\tau^{-1}\right)\frac{\mathrm{d}R_o}{\mathrm{d}t}\,\mathrm{d}R_o. \tag{5.9}$$

https://doi.org/10.1017/S0022112005006208 Published online by Cambridge University Press

a_e/R^*	λ
0.95	1.1
0.66	1.6
0.50	1.9
0.33	2.5
0.05	5.2

TABLE 1. Results from the analysis of the integral in (5.13).

We add now the two expressions (5.8) and (5.9) to obtain

$$0.33V^2\left(\frac{a_e^3}{R_m^3}-\frac{a_e^3}{(R^{\#})^3}\right)-0.18V^2\left(\frac{l^2}{R_m^2}-\frac{l^2}{(R^{\#})^2}\right)$$
$$=\int_{a_e}^{R^{\#}}\left(0.22\frac{Vl^2}{R_o^3}-\tau^{-1}\right)\frac{\mathrm{d}R_o}{\mathrm{d}t}\,\mathrm{d}R_o-\int_{a_e}^{R_m}\left(0.22\frac{Vl^2}{R_i^3}-\tau^{-1}\right)\frac{\mathrm{d}R_i}{\mathrm{d}t}\,\mathrm{d}R_i. \quad (5.10)$$

This is an interesting relation. We have seen that without the horseshoe vortex $R^{\#}$ is always smaller than R_m, because of viscous dissipation. This follows also from (5.10) if we take out the terms with l^2. In the presence of the vortex $R^{\#}$ may be larger than R_m. This means that the outward motion of the bubble stops at a value of R_o beyond where the inward motion started. The inward motion then starts from this value, $R^{\#}$. The process repeats itself until $R_m = R^{\#}$, upon which the two bubbles remain oscillating with that value of R_m. After 50 or so oscillations we are on the time scale of the spiralling motion and this takes over. To see whether such a scheme is possible, we look for values of a_e/R_m where $R_m = R^{\#}$. Anticipating that this value is of order unity, we neglect the terms containing l^2 on the left-hand side of (5.10). Both for the inward and for the outward motion the attractive dipole force is dominant and we can use as a first approximation for $\mathrm{d}R_o/\mathrm{d}t$ and $\mathrm{d}R_i/\mathrm{d}t$ the expressions in (5.6). Inserting this in the integrals in (5.10) it follows that we need to investigate whether

$$\int_{a_e}^{R_m}\left(0.22\frac{Vl^2}{R^3}-\tau^{-1}\right)\left(\frac{R_m^3}{R^3}-1\right)^{1/2}\mathrm{d}R=0, \quad (5.11)$$

for a value of a_e/R_m smaller than one. For brevity and using (3.15) we introduce λ as

$$\lambda = 0.22\frac{Vl^2\tau}{a_e^3}=0.08\frac{V\tau}{a_e}. \quad (5.12)$$

We denote the particular value of R_m for which (5.11) holds by R^*. For that value of R_m the force exerted by the horseshoe vortex is large enough to enable a repeating cycle. In order to solve (5.11) at given λ for a_e/R^* we write $x = R/R^*$ and $a_e/R^* = \zeta$. Inserting this into (5.11) and using (5.12) gives

$$\int_{\zeta}^{1}\left(\frac{\lambda\zeta^3}{x^3}-1\right)\left(\frac{1-x^3}{x^3}\right)^{1/2}\mathrm{d}x=0. \quad (5.13)$$

Solution, see Appendix D, results in the given in table 1 values for a_e/R^* for a number of given λ values. De Vries (2001) measured, for a bubble of radius of 1–1.5 mm, a rise velocity of roughly $0.35\,\mathrm{m\,s^{-1}}$. This in agreement with earlier measurements by Duineveld (1995). The kinematic viscosity of the water in which De Vries (2001) did his experiments was $0.8\times10^{-6}\,\mathrm{m^2\,s^{-1}}$. When we calculate λ for these circumstances

https://doi.org/10.1017/S0022112005006208 Published online by Cambridge University Press

we find 1.57, 1.73 and 1.87 for bubbles with radius 1, 1.25 and 1.5 mm respectively. Table 1 then tells us that R^*/a values can be expected to be of modest magnitude, between 1 and 2.

The above calculation shows that in the configuration of figure 3, with the line of centres horizontal and the horseshoe positioned as in that figure, the bubbles will oscillate indefinitely, with R^* following from the appropriate value of λ.

We verified this by a numerical solution of (5.4) and (5.5) for the case $V\tau/a_e = 20$, corresponding to a bubble of radius $a_e = 1.23$ mm rising in water, $V = 0.28\,\mathrm{m\,s^{-1}}$, with $\nu = 0.8 \times 10^{-6}\,\mathrm{m^2\,s^{-1}}$. The oscillations without trailing vortices beginning with $R_m/a_e = 4$, are shown in figure 7(a). They clearly decay in about twenty oscillations. Figure 7(b) shows the influence of the trailing vortices. Now, as predicted, an equilibrium is reached at R^*/a very close to 1.52, which is the value from our analysis, as table 1 shows, for $\lambda = 1.6$ associated with $V\tau/a_e = 20$ from (5.12). We recall that for this relative motion, induced by another bubble, we have frozen the position in the spiralling motion. From the observations of Ellingsen & Risso (2001) it follows that the sideways excursion in the spiralling motion is relatively small. They used bubbles of radius $a_e = 1.25$ mm. The observed spiralling frequency is about 5 Hz, and the horizontal velocity in the spiralling motion on the average $5\,\mathrm{cm\,s^{-1}}$. De Vries (2001) reports that during the spiralling motion the two threads are not twisted (as suggested by Ellingsen & Risso 2001) and that the vortex force on the bubble itself, i.e. in our example the force by the horseshoe on bubble B is always directed towards the centreline of the spiral.

In the configuration of figure 3 the vortex enables relative motion. However, if the velocity induced by the horseshoe vortex in the centre of A were from right to left, then the analysis points out that the relative motion is even more damped than in the absence of the vortex. Roughly speaking we can assume that, with the line of centres horizontal, half of the time the mutual oscillations between two bubbles are reinforced by the trailing vortices. During this the vector $\boldsymbol{l}$ connecting the arms of the horseshoe is not always at right angles with $\boldsymbol{R}$ as in the above analysis. In the general case in which these enclose an angle ψ the velocity induced in the bubble centre by the vortex is, see (3.22), $\{\Gamma 1/(8\pi \mathrm{R}^2)\}\sin\psi$. This means that the force $F_{2,1}$ in (3.12) must be multiplied with $\sin\psi$, and as a consequence λ takes instead of the right-hand side of (5.12) the value

$$\lambda' = 0.08(V\tau/a_e)\sin\psi = \lambda\sin\psi. \tag{5.14}$$

In the next section we investigate the average intensity of the vortex-induced velocity fluctuations.

6. Intensity of velocity fluctuations

We mentioned in the Introduction that according to the studies of Yurkovetsky & Brady (1996) and Spelt & Sangani (1998) a suspension rising under buoyancy is stable provided velocity fluctuations of the bubbles are sufficiently intense. These authors introduced a virtual temperature T defined as

$$T = (\langle \boldsymbol{v}\cdot\boldsymbol{v}\rangle - \langle \boldsymbol{v}\rangle^2)/3, \tag{6.1}$$

where $\langle\ \rangle$ denotes ensemble averaging. This temperature must exceed some critical value in order to prevent clustering.

It is therefore of interest to calculate that intensity in our case, that is in the presence of horseshoe vortices. The fluctuations are due to the spiralling motion itself,

https://doi.org/10.1017/S0022112005006208 Published online by Cambridge University Press

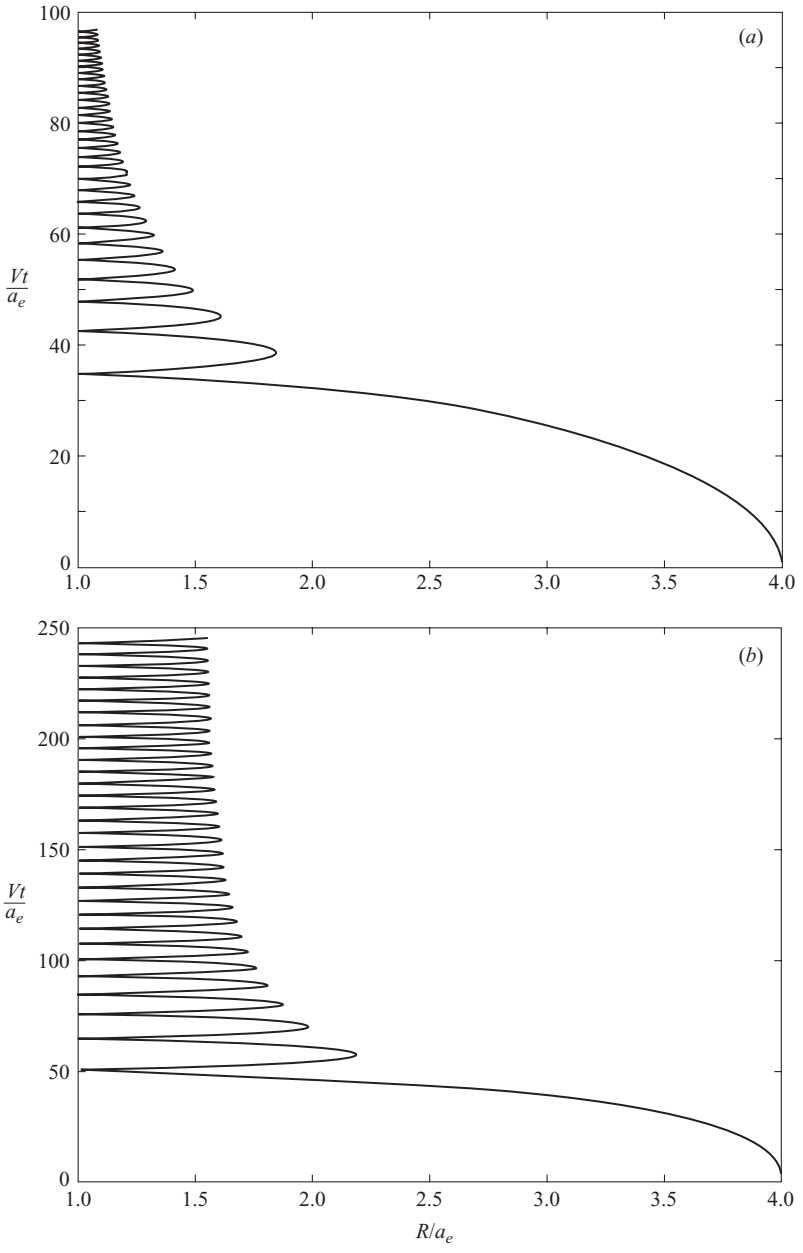

FIGURE 7. Trajectory of one bubble in a pair under the influence of the other. $\lambda = 1.6$. Shown is the ratio R/a_e as a function of the dimensionless elapsed time Vt/a_e. (*a*) Only hydrodynamic attraction by the other bubble in the pair and viscous resistance; (*b*) Trailing vortices behind the other bubble included.

$\boldsymbol{v}_{sp}$, and in addition there are the oscillations studied in the foregoing sections, $\boldsymbol{v}_{hs}$, say, the subscript referring to 'horseshoe'. Hence we can write for the bubble velocity

$$\boldsymbol{v} = V\boldsymbol{i} + \boldsymbol{v}_{sp} + \boldsymbol{v}_{hs}. \tag{6.2}$$

https://doi.org/10.1017/S0022112005006208 Published online by Cambridge University Press

Here $\boldsymbol{i}$ is a unit vector in the vertical direction. The spiralling motion produces mainly horizontal bubble velocities (Ellingsen & Risso 2001). With a bubble of radius a_e they report that in the horizontal plane the trajectory of a spiralling bubble can be represented by an excursion X, where

$$X \approx 3.2 a_e \sin 2\pi f t, \tag{6.3}$$

f being the spiral frequency, about 5 Hz. Similar figures are provided by de Vries (2001). We introduce the number density of the bubbles n and their concentration by volume α as

$$\alpha = (4/3)\pi n (a_e)^3. \tag{6.4}$$

Then, taking into account the bubble volume, we have from (6.3) and (6.4)

$$\langle \boldsymbol{v}_{sp} \cdot \boldsymbol{v}_{sp} \rangle \approx 200 \alpha (a_e)^2 f^2. \tag{6.5}$$

Next we consider $\langle \boldsymbol{v}_{hs} \cdot \boldsymbol{v}_{hs} \rangle$. To have an idea about the quantities involved, consider the mutual oscillations of two bubbles which we have investigated in the foregoing sections. If we compare these with the spiralling motion, we note first that the frequency is of order V/a_e, much higher than f. Whereas the amplitude of the spiralling motion is of order a_e, it is of order R_m for the oscillation due to hydrodynamic interaction. Hence the ratio of $\langle \boldsymbol{v}_{hs} \cdot \boldsymbol{v}_{hs} \rangle$ to the right-hand side of (6.5) is of order

$$10^{-2} \frac{V^2}{(a_e f)^2} \langle R_m^2 \rangle / (a_e)^2. \tag{6.6}$$

This is a large quantity, of order 10^2.

We consider a large number, N, of bubbles in a large volume E. The ensemble average of a quantity G, say, is defined as

$$\langle G \rangle = \int G(C_N, \dot{C}_N) P(C_N, \dot{C}_N / \boldsymbol{x}) \, \mathrm{d}C_N \, \mathrm{d}\dot{C}_N, \tag{6.7}$$

where C_N and $\dot{C}_N$ indicate the configuration space and the velocity space of N bubbles, and $P(C_N, \dot{C}_N/\boldsymbol{x}) \, \mathrm{d}C_N \, \mathrm{d}\dot{C}_N$ is the probability of finding another bubble in an element of that space given that there is a bubble in $\boldsymbol{x}$. Assuming that all quantities involved fall off sufficiently rapidly we may, for dilute suspensions, restrict considerations to interactions between pairs. As in the foregoing sections, we will consider pairs separated by a distance $2\boldsymbol{R}$ and having a relative velocity $2\dot{\boldsymbol{R}}$. Instead of $\dot{\boldsymbol{R}}$ we employ $\boldsymbol{R}_m$ related to $\boldsymbol{R}$ and $\dot{\boldsymbol{R}}$ by a relation of the type (5.6). Since the distance between the test bubble in $\boldsymbol{x}$ and another bubble is $2\boldsymbol{R}$, we introduce

$$\boldsymbol{S} = 2\boldsymbol{R}, \quad \boldsymbol{S}_m = 2\boldsymbol{R}_m. \tag{6.8}$$

In principle P is the solution of a Liouville equation which can be solved once the trajectories of bubbles are known. With viscous potential flow around bubbles no steady solution of that Liouville equation exists, as shown in VW. All bubbles cluster at $S_m = 2a_e$. Here we know that, depending on λ' (defined by (5.14)) various steady-state values of S_m exist. In order to make an estimate of the value of T obtained in this way, we make some assumptions on P. We introduce both for $\boldsymbol{S}$ and $\boldsymbol{S}_m$ spherical polar coordinates S, β, ψ and S_m, β_m, ψ_m respectively. The elements of volume in $\boldsymbol{S}$ and $\boldsymbol{S}_m$ space are thus $S^2 \sin\beta \, \mathrm{d}\beta \, \mathrm{d}\psi \, \mathrm{d}S$ and $S_m^2 \sin\beta_m \, \mathrm{d}\beta_m \, \mathrm{d}\psi_m \, \mathrm{d}S_m$ respectively. At given values of $\boldsymbol{x}$ and $\boldsymbol{S}_m$ the probability of finding a bubble in $\boldsymbol{S}$ is independent of ψ but the probability for β near $\pi/2$ is very high (see VW). We shall use this in the following.

https://doi.org/10.1017/S0022112005006208 Published online by Cambridge University Press

Integration of $P(\boldsymbol{S}|\boldsymbol{x})$, for all $\boldsymbol{S}_m$ together, must give $N-1$, equal to N for large N. We take for the present purpose, using the number density $n = N/E$,

$$\begin{aligned} P(S, \beta|\boldsymbol{x}) &= 0, S \leqslant 2a \\ &= n\delta(\beta - \pi/2), S > 2a. \end{aligned} \tag{6.9}$$

In (6.9) δ is the Delta function. We could have taken another expression to indicate the strong preference for lines of centres at right angles with the vertical direction, but this would not influence the result much because we will integrate over β. Because integration of P over $\boldsymbol{S}$ and $\boldsymbol{S}_m$ must give the total number of bubbles and because of the choice (6.9) $P(\boldsymbol{S}_m)$ is subject to the condition

$$\int P(\boldsymbol{S}_m)\,\mathrm{d}\boldsymbol{S}_m = 1. \tag{6.10}$$

After these preliminaries we consider the average $\langle \boldsymbol{v}_{hs} \cdot \boldsymbol{v}_{hs} \rangle$. In the preceding sections we have considered the case in which the line of centres of the two bubbles is horizontal. We consider now the general case. Take a plane through the line of centres and the vertical and let the angle between the vertical and the line of centres be β. For the velocity $\dot{\boldsymbol{R}}$ of each of the bubbles in a pair we take as an approximation the velocity in the absence of viscosity and also in the absence of the horseshoe vortices. This is justified by both the viscous force and the force induced by the vortices being small with respect to the attraction by the other bubble. The relative motion then is entirely in that plane. Consider expression (3.9) applied to the force exerted on the dipole in B on the test bubble. This force can be written as the gradient of a potential Φ, say, where

$$\Phi = -4\pi\rho \boldsymbol{M} \cdot \nabla(\boldsymbol{M} \cdot \boldsymbol{S}/S^3). \tag{6.11}$$

The dipole strength $\boldsymbol{M}$ has components given in (3.7) and (3.8):

$$4\pi\boldsymbol{M} = Y[\{1 + Q_1(2)\}V\boldsymbol{i} + \{1 + Q_2(2)\dot{\boldsymbol{R}}]. \tag{6.12}$$

Potential energy is converted into kinetic energy during the oscillation. In VW the case of spheres is treated and it is shown there that the contribution to the kinetic energy by the term with $\dot{\boldsymbol{R}}$ in (6.12) is negligibly small. This is even more the case for oblate ellipsoids since $Q_2(2)$ is only 0.30, whereas $Q_1(2)$ has the value 1.17, both having the value 0.5 for spheres. Leaving only the first term on the right-hand side of (6.12), inserting the above-mentioned values for Q_1 and Q_2 in (6.11) gives

$$\Phi = -\frac{2.15\pi\rho a_e^6 V^2(1 - 3\cos^2\beta)}{S^3}. \tag{6.13}$$

The maximum value is obtained when the two bubbles have their largest distance S_m apart. The kinetic energy involved in the relative motion is the difference between this maximum value of Φ and the value at intermediate S and β. This is the kinetic energy for A and B together, $\boldsymbol{v}_{hs} \cdot \boldsymbol{v}_{hs}$, times the added mass. Since in the general case the relative velocity has components both in the S- and in β-directions here we take for Q the value 0.5 for a sphere. Then it follows from (6.13) that

$$\boldsymbol{v}_{hs} \cdot \boldsymbol{v}_{hs} = 3.23 a_e^3 V^2 \left\{ \frac{1}{S^3} - \frac{1}{S_m^3} - 3\left(\frac{\cos^2\beta}{S^3} - \frac{\cos^2\beta_m}{S_m^3} \right) \right\}. \tag{6.14}$$

From (6.1), (6.2) and (6.14) it follows that we have to average 1/3 of the expression on the right-hand side of (6.14). This means integration over the $\boldsymbol{S}$, $\boldsymbol{S}_m$ space, the

https://doi.org/10.1017/S0022112005006208 Published online by Cambridge University Press

elements of which are given above (6.9). We start with integration over β which gives as integrand

$$1.08a_e^3V^2\{S^{-3}-S_m^{-3}(1-3\cos^2\beta_m)\}\sin\beta_m\,\mathrm{d}\beta_m. \tag{6.15}$$

Analysis of the trajectories given by (6.11) and (6.12) shows, see e.g. Kok (1993*a*), that the oscillations we are interested in occur for angles β_m such that

$$|\cos\beta_m|<3^{-1/2}. \tag{6.16}$$

For other directions the main hydrodynamic force (see also (6.13)) is repulsive and the bubbles are soon out of each other's reach. We introduce therefore

$$\beta^*=\cos^{-1}1/\sqrt{3} \tag{6.17}$$

and integrate the expression in (6.15) between β^* and $\pi-\beta^*$,

$$1.08a_e^3V^2\int_{\beta^*}^{\pi-\beta^*}\left\{\frac{1}{S^3}-\frac{1}{S_m^3}(1-3\cos^2\beta_m)\right\}\sin\beta_m\,\mathrm{d}\beta_m=1.24a_eV^3\left(\frac{1}{S^3}-\frac{2}{3S_m^3}\right). \tag{6.18}$$

We multiply the right-hand side of (6.19) with $\pi nS^2\,\mathrm{d}S$ and integrate over S. The probability distribution $P(\boldsymbol{S}_m)$ is reduced to $P(S_m,\psi)$ since we have already integrated over β. Using (6.10) and the expression (6.4) for the relation between number density n and volume concentration α we obtain for the average kinetic energy of the vortex-induced fluctuations

$$T=0.93\alpha V^2\int\mathrm{d}\psi\int P(S_m,\psi)\left[\ln\frac{S_m}{2a}-\frac{2}{9}\left\{1-\left(\frac{2a}{S_m}\right)^3\right\}\right]S_m^2\,\mathrm{d}S_m. \tag{6.19}$$

We know that $P(S_m,\psi)$ must obey (6.10). Further we know that in the steady state two possible values of S_m remain. For values of ψ such that $0.08\,V\tau/a\sin\psi>1$, see (5.14), $S_m/2a>1$. At other values of ψ oscillations decay to $S_m=2a$. We have denoted the equilibrium value of S_m in the first category by $2R^*$. If we in addition denote the value of ψ at which (cf. (5.14)) $\lambda'=1$ with ψ^*, and take (6.10) into account, we have for $P(S_m,\psi)$,

$$\begin{aligned}P(S_m,\psi)&=\frac{\pi-2\psi^*}{\pi}\frac{\delta(S_m-2a_e)}{S_m^2}\qquad\text{for}\quad\sin\psi\leqslant\lambda^{-1},\\&=\frac{2\psi^*}{\pi}\frac{\delta(S_m-2R^*)}{S_m^2}\qquad\text{for}\quad\lambda^{-1}<\sin\psi\leqslant1.\end{aligned} \tag{6.20}$$

We now insert (6.20) into (6.19) and obtain finally, taking (6.1), (6.2) and (6.5) into account,

$$T=\left(\frac{\langle\boldsymbol{v}\cdot\boldsymbol{v}\rangle^2-\langle\boldsymbol{v}\rangle^2}{3}\right)=200\alpha a_e^2f^2+1.18\psi^*\alpha V^2\int_{\psi^*}^{\pi/2}\left\{\ln\frac{R^*}{a_e}-\frac{2}{9}\left(1-\frac{a_e^3}{R^{*3}}\right)\right\}\mathrm{d}\psi. \tag{6.21}$$

Equation (6.21) is the main result of this investigation. The effective bubble temperature T, defined (cf. (6.1)) as the intensity of the bubble velocity fluctuations, has two contributions, one from the spiralling motion of the bubbles, the first term on the right-hand side of (6.21) and the remainder due to hydrodynamic interaction with neighbours, and sustained by trailing vortices. Since $(a_ef/V)^2$ for a bubble of radius 1 mm and a spiralling frequency of 6, say, is of order $(10)^{-4}$, the contribution of the spiralling motion is relatively small, as anticipated earlier in this paper. The other terms contain R^*, the amplitude at which a stable oscillation of one bubble with

https://doi.org/10.1017/S0022112005006208 Published online by Cambridge University Press

respect to another can be maintained through the action of the trailing vortices, and depending on ψ through (5.14) and the results in table 1.

To see what kind of temperatures (6.21) gives, we take an example from the measurements of de Vries (2001). He measured in water with kinematic viscosity $\nu = 0.8 \times 10^{-6}\,\mathrm{m^2\,s^{-1}}$ a velocity V of about $0.30\,\mathrm{m\,s^{-1}}$ with a bubble of radius $a_e = 1.20 \times 10^{-3}\,\mathrm{m}$. Using (5.2), (5.12) and (5.14) we find $\lambda = 1.7$, giving $\sin\psi^* = 0.59$, or $\psi^* = 0.55$ rad. At this angle R^*/a_e has a minimum value 1 and rises to 1.7 at $\psi = \pi/2$. It follows from the values in table 1 and from (5.14) that between these values the relation between R^*/a_e and ψ is very well represented by

$$R^*/a_e = 2\sin\psi. \tag{6.22}$$

Inserting this in (6.23) gives for these bubbles

$$T = 0.21\alpha V^2 + 200\alpha(a_e f)^2 = 0.24\alpha V^2. \tag{6.23}$$

It is hard to say whether this is sufficient to prevent clustering of bubbles. In the next section we shall discuss our result in the light of the scarce literature on this issue.

7. Comparison with other work

We have estimated the velocity variance, expressed as a temperature T, induced by trailing vortices bearing in mind the idea that such velocity fluctuations might be able to prevent bubble clustering. The importance of bubble velocity fluctuations in preventing clustering is clearly demonstrated in the numerical studies by Yurkovetsky & Brady (1996) and Spelt & Sangani (1998). In both of these simulations the flow is essentially potential. In the first the flow is fully potential, in the latter it is viscous potential flow, including dissipation. This means that in neither of these simulations does the wake play a role. Clustering occurs in both simulations below a certain temperature. It should be stressed that it is essentially an inertial effect. Indeed, Smereka (1993) showed that in potential flow bubbles tend to maximize their virtual mass, which happens in horizontal clusters. It is, as is shown in the present paper, further enhanced by viscous dissipation. Yurkovetsky & Brady (1996) treat the bubbly suspension as condensed matter and determine, employing statistical mechanics, a phase transition where the suspension changes from the fluid phase in a solid phase. Their estimate of the associated critical temperature T_c is, in terms of the symbols of the present paper,

$$T_c/V^2 = 0.015\alpha. \tag{7.1}$$

Spelt & Sangani (1998) calculate, describing the relative flow between bubbles and liquid as a viscous potential flow, the stress distribution due to hydrodynamic interaction. They determine the trace of this stress and call it the particle pressure. This consists of a kinetic part, increasing with T, and a hydrodynamic part, which is always negative. They propose as a reasonable criterion for the occurrence of clustering the temperature at which this particle pressure becomes zero. This leads to

$$T_c/V^2 = 2.25\alpha. \tag{7.2}$$

Since the criteria leading to (7.1) and (7.2) are so widely different it is difficult to compare these with one another or with our result exemplified by (6.23). At most one could expect that the temperature needed to prevent clustering should be somewhat higher when viscous dissipation is allowed for. In spite of their limited significance for the present work, these few results should be mentioned.

https://doi.org/10.1017/S0022112005006208 Published online by Cambridge University Press

Interesting experimental data on bubble velocity variance and bubble clustering were reported in Zenit, Koch & Sangani (2001) and in Kusch *et al.* (2002). In the former paper it was reported that the measured values of T/V^2 in bubbly suspensions rising in a vertical channel were "about a factor 5 smaller than those [the criterion of Spelt and Sangani, cf (7.2)] necessary to stabilise the suspension". In the later paper by Kusch *et al.* it was in addition reported that the expression

$$T/V^2 = 0.02 + 0.5\alpha. \tag{7.3}$$

fits the measurements by Zenit *et al.* (2001) very well.

In the above-mentioned papers pictures of the bubbles are shown. It appears that on average the diameter is slightly more than 2 mm. According to the experiments done by de Vries (2001) spiralling starts at $a_e = 0.8$ mm. Hence the bubbles in the experiments by Zenit *et al.* (2001) are spiralling. It is hard to understand the term 0.02 on the right-hand side of (7.3), since it would mean bubble velocity fluctuations even if there were no bubbles, but the authors attribute this to phenomena at very low concentration and associated with wall effects. Apart from this term the experimental results summarized in (7.3) are close to our theoretical value of T in (6.23) for bubbles with $a_e = 1.20$ mm.

8. Conclusion

We have investigated pair interactions between bubbles in a liquid. The primary force is the attraction or repulsion caused by the potential flow about a neighbour. It is well known that clustering occurs in simulations of suspensions under these conditions. We have considered the possibility that additional forces caused by trailing vortices may supply energy to the relative motion and thereby lead to persistence of the latter.

The trailing vortices, as they have been observed in experiments and in numerical flow simulations by others, are here modelled as horseshoe vortices.

A concise summary of the present work is in fact equation (5.10) expressing that sustained stirring (left-hand side) is possible provided the average work by the vortices is larger than the viscous dissipation in the relative motion (right-hand side). The preceding analysis is needed to derive this relation and, in particular, to give justification to a number of simplifying assumptions and approximations.

It appears from our calculations that these vortices can indeed lead to velocity fluctuations of bubbles. At this moment it is, in view of the paucity of a data (only numerical simulations of a different nature are available), not possible to predict whether these fluctuations are sufficiently intense to prevent clustering.

I am grateful to Arie Biesheuvel, Detlef Lohse and Andrea Prosperetti for their comments on an earlier draft of the paper. I thank Christian Veldhuis and Gerrit de Bruin for their help with the numerical computation, and one of the referees for his comments, in particular for strongly suggesting treating ellipsoidal shapes instead of a spherical approximation.

Appendix A. Calculation of the force on the image of the horseshoe vortex in the bubble

We start with the force $\boldsymbol{F}_3$, say, on the vortex ring in the plane through the origin and the semi-infinite line vortex $-\infty < x < 0$, $y = -l/2$, $z = 0$, with circulation $-\Gamma$. In

https://doi.org/10.1017/S0022112005006208 Published online by Cambridge University Press

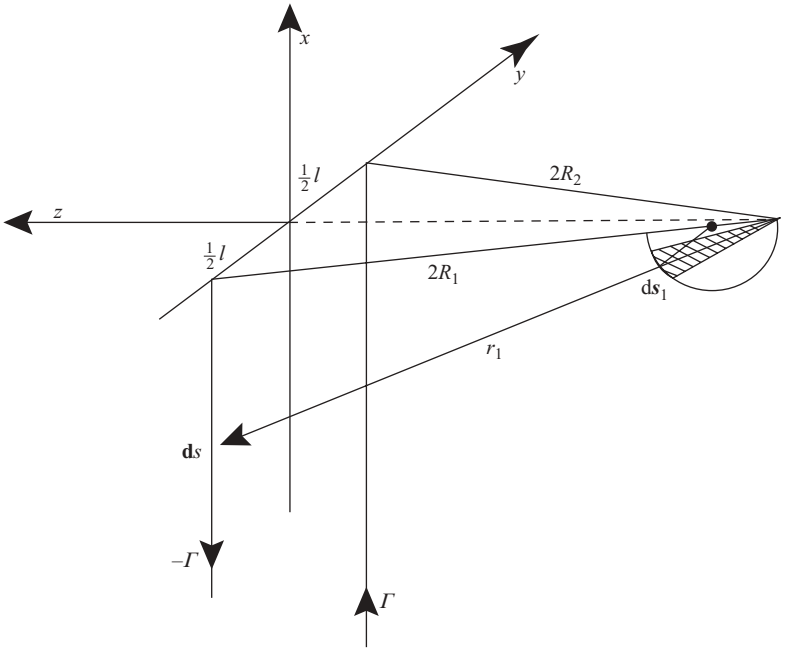

FIGURE 8. Shown is the horseshoe vortex of bubble B and the image of one of the arms, $-\infty < x < 0$, $y = -l/2$, $z = 0$, in bubble A.

figure 8 this plane is sketched including the vortex ring with element $\mathrm{d}\boldsymbol{s}_1$, the radius vector $\boldsymbol{r}_1$ of an element $\mathrm{d}\boldsymbol{s}$ of the line vortex the starting point of which is at a distance $2R_1$ from the origin of bubble A. We are interested in the force in the z-direction, $\boldsymbol{F}_3 \cdot \boldsymbol{e}_z$,

$$\boldsymbol{F}_3 \cdot \boldsymbol{e}_z = \rho \boldsymbol{e}_z \cdot \int (\boldsymbol{u} \times \boldsymbol{\omega})\, \mathrm{d}\Omega, \tag{A 1}$$

where Ω the volume occupied by the vortex ring and ω denotes vorticity. We have

$$\boldsymbol{\omega}\, \mathrm{d}\Omega = -\Gamma r_1/a\, \mathrm{d}\boldsymbol{s}_1. \tag{A 2}$$

With reference to figure 8 and with θ and ϕ as indicated in figure 6, we have $r_1 = 2R_1/\cos\theta_1$ and $\mathrm{d}\boldsymbol{s}_1 = a^2/4R_1 \boldsymbol{e}_{\varphi 1}\, \mathrm{d}\phi_1$. Using these results and, from geometry, $\phi_1 = 2\theta_1$ we obtain for (A 2)

$$\boldsymbol{\omega}\, \mathrm{d}\Omega = -\Gamma a \boldsymbol{e}_{\phi 1}\, \mathrm{d}\phi_1/2\cos(\phi_1/2). \tag{A 3}$$

Interestingly, this result does not depend on R_1. That means that we can write down the same expression for the corresponding force $\boldsymbol{F}_4$ on the other vortex ring, with a change of sign of Γ. Denoting now the velocity induced by the horseshoe vortex, as a whole, at a point of the first vortex ring by $\boldsymbol{u}_1$ and similarly by $\boldsymbol{u}_2$ a point on the second one, with the same $\phi = \phi_1 = \phi_2$, we can write

$$(\boldsymbol{F}_3 + \boldsymbol{F}_4) \cdot \boldsymbol{e}_z = \rho \Gamma a \boldsymbol{k} \cdot \int \{(\boldsymbol{u}_2 \times \boldsymbol{e}_{\varphi,2}) - (\boldsymbol{u}_1 \times \boldsymbol{e}_{\phi,1})\}/2\cos(\phi/2)\, \mathrm{d}\phi. \tag{A 4}$$

The expression between { } can be written as

$$\{(\boldsymbol{u}_2 - \boldsymbol{u}_1) \times \boldsymbol{e}_{\phi,1} + \boldsymbol{u}_1 \times (\boldsymbol{e}_{\phi,2} - \boldsymbol{e}_{\phi,1}) + (\boldsymbol{u}_2 - \boldsymbol{u}_1) \times (\boldsymbol{e}_{\phi,2} - \boldsymbol{e}_{\phi,1})\}. \tag{A 5}$$

https://doi.org/10.1017/S0022112005006208 Published online by Cambridge University Press

We investigate the contribution of each of the above terms to the integral in (A 4). We start with the second term which gives, as will turn out, the largest contribution. For x and y of order l and z of order $2R$, which holds for points on the vortex rings, u is, see (3.11)–(3.13) of order $(\Gamma/2\pi)(l/(2R)^2)$. Further $|\boldsymbol{e}_{\phi,2}-\boldsymbol{e}_{\phi,1}|$ is of order $l/2R$. Introduced in (A 4) this results in $\rho\Gamma^2 al^2/16\pi R^3$. Using the expression (3.18) for Γ and taking as before $U=0.2V$, this given

$$0.04\pi\rho V^2 l^4 a/R^3. \tag{A 6}$$

This is 0.40 $(l/a)^2$ times the right-hand side of (3.20) (with $Q_1=0.5$) and 0.40 $(l/a)^2(V/|\dot{\boldsymbol{R}}|)$ times the right-hand side of (3.19), which makes the contribution (A 6) to the force negligibly small.

Next we consider the contribution of the first term in (A 5) to the integral in (A 4). Take points with the same value of ϕ on each of the two vortex rings. They are separated by a distance of order $la^2/4R^2$. This is mainly in the y-direction of the coordinates x, y, z in terms of which the velocity components of $\boldsymbol{u}$ in (3.11)–(3.13) are given. For a point with x and y of order l and z of order $2R$, we find that, for example, $\partial u_x/\partial y$ is of order $\Gamma/4\pi\, l^2/(2R)^4$. Hence for two such points separated in the y-direction by the above-mentioned distance

$$|\boldsymbol{u}_2-\boldsymbol{u}_1| \sim (\Gamma/4\pi)\, l^3 a^2/(2R)^6.$$

Inserting this into (A 4), we find a contribution of order $\rho\Gamma^2 l^3 a^3/\{4\pi(2R)^6\}$ With, as before, $\Gamma=4\pi U l$ and $U=0.2V$, this is

$$0.2\pi\rho V^2 l^5 a^3/(2R)^6.$$

Since $l\approx 0.6a$ and $R\geqslant a$, this is much smaller than either F_2 or F_3 as given in (3.19) and (3.20).

The forces, let us call them $\boldsymbol{F}_6$ and $\boldsymbol{F}_7$, caused by the horseshoe vortex on the vortex sheets, are estimated in a similar way. We start again with looking at the sheet in figure 8. Working out for $\boldsymbol{F}_6$ a relation similar to (A 1), we must evaluate $\boldsymbol{\omega}\,\mathrm{d}\Omega$ for a piece of the sheet. Remembering that the circulation of the pertinent arm of the horseshoe is negative, we use relation (4.1) which gives the circulation per unit length of the radius connecting the origin with the observed point on the vortex ring. The length of this radius is a^2/r_1, giving

$$\omega\,\mathrm{d}\Omega = -\Gamma a/r_1\,\mathrm{d}s_r. \tag{A 7}$$

Now $\mathrm{d}s_r$ is on the arm of the horseshoe vortex and we want this expressed in terms of the corresponding element $\mathrm{d}s_1$ of the vortex ring. The relation is

$$\mathrm{d}s_1 = \frac{\mathrm{d}s_{r1}}{\sin\left(\frac{1}{2}\phi_1\right)} = \frac{a^2}{{r_1}^2\sin\left(\frac{1}{2}\phi_1\right)}\,\mathrm{d}s_r \tag{A 8}$$

Using this and $\mathrm{d}s_1=a^2/4R_1\,\mathrm{d}\varphi_1$, we obtain from (A 7)

$$\boldsymbol{\omega}\,\mathrm{d}\Omega = -\Gamma a r_1/4R_1\sin(\phi_1/2)\,\mathrm{d}\phi_1\boldsymbol{e}_{r,1}.$$

From the geometry in figure 7 we see that $\cos(\varphi_1/2)=2R_1/r_1$, so that we finally have

$$\boldsymbol{\omega}\,\mathrm{d}\Omega = -2\Gamma a\tan(\phi_1/2)\,\mathrm{d}\phi_1\boldsymbol{e}_{r,1}. \tag{A 9}$$

The calculation of the corresponding force leads to an integral similar to the one on the right-hand side of (A 4), with $\boldsymbol{e}_{r,1}$ and $\boldsymbol{e}_{r,2}$ instead of $\boldsymbol{e}_{\phi,1}$ and $\boldsymbol{e}_{\phi,2}$ respectively. The outcome is therefore of the same order of magnitude as (A 6).

https://doi.org/10.1017/S0022112005006208 Published online by Cambridge University Press

The reader might wonder about the apparent singularity in (A 4) when $\phi = \pi$. However, the product of $\{(\cos(\phi/2)\}^{-1}$ both with $|(\boldsymbol{u}_2 - \boldsymbol{u}_1)|$ and with $|(\boldsymbol{e}_{\phi,2} - \boldsymbol{e}_{\phi,1})|$ remains finite when ϕ approaches π.

Appendix B. Motion of horseshoe vortex behind bubble *B*, caused by that behind *A*

We consider the displacement in the z-direction in figure 3 of the trailing vortices behind the test bubble A as caused by its counterpart behind bubble B. Equation (3.13) of the main text gives for the induced velocity in that direction, at $x = 0$ of figure 3, where the vortices are located,

$$u_z = -\frac{\Gamma}{4\pi}\left\{\frac{y - \frac{1}{2}l}{z^2 + \left(y - \frac{1}{2}l\right)^2} - \frac{y + \frac{1}{2}l}{z^2 + \left(y + \frac{1}{2}l\right)^2}\right\}. \tag{B 1}$$

For $z = -3a_e$ (the example in figure 7*b*), we have at $y = l/2$ and $y = -l/2$, where the vortices are,

$$u_z = -\frac{\Gamma l}{4\pi\left(9a_e^2 + l^2\right)}. \tag{B 2}$$

Using the relations (3.15) and (3.18) in the main text, we find from (B 2)

$$u_z = -0.04U,$$

which is quoted in the main text.

Appendix C. Added mass of ellipsoids

Milne-Thomson (1968, p. 501) gives the added mass m_1 for acceleration in the direction of the minor axis of an axisymmetric ellipsoid expressed in terms of the ratio of major to minor axis χ as $\rho Y Q_1$, where

$$Q_1(\chi) = \frac{(\chi^2 - 1)^{1/2} - \cos^{-1}\chi^{-1}}{\cos^{-1}\chi^{-1} - (\chi^2 - 1)^{1/2}\chi^2}. \tag{C 1}$$

This result is obtained by calculating an integral, where a and b are the minor and major axes respectively,

$$\alpha_0 = ab^2 \int_0^{\infty} \frac{\mathrm{d}\lambda}{(a^2 + \lambda)^{3/2}(b^2 + \lambda)}. \tag{C 2}$$

The relation between Q_1 and α_0 is

$$Q_1 = \frac{\alpha_0}{2 - \alpha_0}. \tag{C 3}$$

Likewise Q_2 in (3.2) in the main text is related to a quantity β_0 by

$$Q_2 = \frac{\beta_0}{2 - \beta_0}, \tag{C 4}$$

where

$$\beta_0 = ab^2 \int_0^{\infty} \frac{\mathrm{d}\lambda}{(a^2 + \lambda)^{1/2}(b^2 + \lambda)^2}. \tag{C 5}$$

https://doi.org/10.1017/S0022112005006208 Published online by Cambridge University Press

Partial integration of the integral in (C 5) gives $\beta_0 = 1 - \alpha_0/2$, whence with the help of (C 3)–(C 5) we obtain

$$Q_2 = \frac{1}{1+2Q_1}. \tag{C 6}$$

Appendix D. Analytic solution of the integral in (5.13)

Consider the integral in (5.13) of the main text

$$\int_\varsigma^1 \left(\frac{\lambda\varsigma^3}{x^3} - 1\right)\left(\frac{1-x^3}{x^3}\right)^{1/2} \mathrm{d}x = 0.$$

We write $\lambda\varsigma^3/x^3$ as $\lambda\varsigma^3(1-x^3+x^3)/x^3$ and use the result

$$\int_\varsigma^1 \frac{(1-x^3)^{3/2}}{x^{9/2}}\,\mathrm{d}x = \frac{2}{7}\left[\frac{(1-\varsigma^3)^{3/2}}{\varsigma^{7/2}} - \frac{9}{2}\int_\varsigma^1 \frac{(1-x^3)^{1/2}}{x^{3/2}}\,\mathrm{d}x\right],$$

to obtain

$$\frac{\lambda}{(7+2\lambda\varsigma^3)(1-\varsigma^3)^{3/2}} = (1-\varsigma^3)^{1/2} - \frac{3}{2}\varsigma^{1/2}\int_\varsigma^1 \frac{x^{3/2}}{(1-x^3)^{1/2}}\,\mathrm{d}x. \tag{D 1}$$

The integral on the right-hand side of (D 1) can be expressed as an incomplete Beta function which is useful for checking a numerical calculation for ζ values close to zero or one. Abramowitz & Stegun (1970, p. 258) give

$$\int_\zeta^1 \frac{x^{3/2}}{(1-x^3)^{1/2}} = \frac{1}{3}\int_\xi^1 \frac{\mathrm{d}y}{(1-y)^{1/2}y^{1/6}} = \frac{1}{3}B\left(\frac{5}{6},\frac{1}{2}\right) - \frac{1}{3}B_\xi\left(\frac{5}{6},\frac{1}{2}\right) \quad \text{with } \xi = \zeta^3. \tag{D 2}$$

Table 1 in the main text is obtained from numerical integration and (D 1).

REFERENCES

Abramowitz, M. & Stegun, I. 1970 *Handbook of Mathematical Functions*. Dover.

Benjamin, T. B. & Ellis, A. T. 1990 Self-propulsion of asymmetrically vibrating bubbles. *J. Fluid Mech.* **212**, 65–80.

Cartellier, A. & Rivière, N. 2001 Bubble-induced agitation and microstructure in uniform bubbly flows at small to moderate particle Reynolds numbers. *Phys. Fluids* **13**, 2165–2181.

Dhanak, M. R. 1981 Interaction between a vortex filament and an approaching rigid sphere. *J. Fluid Mech.* **110**, 129–147.

Duineveld, P. C. 1994 Bouncing and coalescence of two bubbles in water. PhD Thesis, University of Twente, Enschede.

Duineveld, P. C. 1995 The rise velocity and shape of bubbles in pure water at high Reynolds numbers. *J. Fluid Mech.* **292**, 325–332.

Duineveld, P. C. 1998 Bouncing and coalescence of bubble pairs rising at high Reynolds number in Pure Water or Aqueous Surfactant Solutions. *Appl. Sci. Res.* **58**, 409–439.

Ellingsen, K. & Risso, F. 2001 On the rise of an ellipsoidal bubble in water: oscillatory paths and liquid induced velocity. *J. Fluid Mech.* **440**, 235–268.

Kok, J. B. W. 1993*a* Dynamics of a pair of gas bubbles moving through liquid; Part 1 Theory. *Eur. J. Mech.* B *Fluids* **12**, 515–541.

Kok, J. B. W. 1993*b* Dynamics of a pair of gas bubbles moving through liquid; Part 2 Experiments. *Eur. J. Mech.* B *Fluids* **12**, 541–560.

Kumaran, V. & Koch, D. L. 1993 The rate of coalescence in a suspension of high Reynolds number, low Weber numbers. *Phys. Fluids* A **5**, 1135–1140.

Kusch, V. I., Sangani, A., Spelt, P. D. M. & Koch, D. L. 2002 Finite-Weber-number motion of bubbles through a nearly inviscid liquid. *J. Fluid Mech.* **460**, 241–280.

https://doi.org/10.1017/S0022112005006208 Published online by Cambridge University Press

Landweber, L. & Miloh, T. 1980 Unsteady Lagally theorem for multipoles and deformable bodies. *J. Fluid Mech.* **96**, 33–46.

Legendre, D., Magnaudet, J. & Mougin, G. 2003 Hydrodynamic interactions between two spherical bubbles rising side by side in a viscous liquid. *J. Fluid Mech.* **497**, 133–166.

Lighthill, M. J. 1956 The image system of a vortex element in a rigid sphere. *Proc. Camb. Phil. Soc.* **52**, 317–321.

Lunde, K. & Perkins, R. J. 1997 Observations on wakes behind spheroidal bubbles and particles. *Paper FEDSM97-3530, ASME-FED* Summer Meeting, Vancouver.

Magnaudet, J. & Eames, I. 2000 The motion of high-Reynolds number bubbles in inhomogeneous flows. *Annu Rev. Fluid Mech.* **32**, 659–708.

Milne-Thomson, L. M. 1952 *Theoretical Aerodynamics.* Macmillan.

Milne-Thomson, L. M. 1968 *Theoretical Hydrodynamics.* Dover.

Moore, D. W. 1963 The boundary layer on a spherical gas bubble. *J. Fluid Mech.* **16**, 161–176.

Moore, D. W. 1965 The velocity of rise of distorted gas bubbles in a liquid of small viscosity. *J. Fluid Mech.* **23**, 749–766.

Mougin, G. & Magnaudet, J. 2002 Path instability of a rising bubble. *Phys. Rev. Lett.* **88**, 014502–014504.

Risso, F. & Ellingsen, K. 2002 Velocity fluctuations in a homogeneous dilute dispersion of high-Reynolds-number rising bubbles. *J. Fluid Mech.* **453**, 395–410.

Sangani, S. & Didwania, A. K. 1993 Dynamic simulations of flows of bubbly liquids at large Reynolds numbers. *J. Fluid Mech.* **250**, 307–337.

Smereka, P. 1993 On the motion of bubbles in a box. *J. Fluid Mech.* **254**, 79–112.

Spelt, P. D. M. & Sangani, A. 1998 Properties and averaged equations for flows of bubbly liquids. *Appl. Sci. Res.* **58**, 337–386.

Stewart, C. W. 1995 Bubble interaction in low-viscosity liquids. *Intl J. Multiphase Flow* **21**, 1037–1046.

Veldhuis C. H. J. & van Wijngaarden, L. 2005 Drag and frequencies of surface oscillations of ellipsoidal bubbles, to be submitted to *J. Engng Maths.*

de Vries, A. W. G. 2001 Path and wake of a rising bubble. PhD Thesis, University of Twente, Enschede, The Netherlands.

de Vries, A. W. G., Biesheuvel, A. & van Wijngaarden, L. 2002 Notes on the path and wake of a gas bubble rising in pure water. *Intl J. Multiphase Flow* **28**, 1823–1835.

van Wijngaarden, L. 1976 Hydrodynamic interaction between gas bubbles in liquid. *J. Fluid Mech.* **77**, 27–44.

van Wingaarden, L. & Kapteyn, C. 1990 Concentration waves in dilute bubble/liquid mixtures. *J. Fluid Mech.* **212**, 111–137.

van Wijngaarden, L. 1993 The mean rise velocity of pairwise-interacting bubbles in liquid. *J. Fluid Mech.* **251**, 55–78 (referred to herein as VW).

Yurkovetsky, Y. & Brady, J. F. 1996 Statistical mechanics of bubbly liquids. *Phys. Fluids* **8**, 881–895.

Zenit, R., Koch, D. L. & Sangani, A. S. 2001 Measurements of the average properties of a suspension of bubbles rising in a vertical channel. *J. Fluid Mech.* **429**, 307–34.

https://doi.org/10.1017/S0022112005006208 Published online by Cambridge University Press